*MRS Communications (2019)*, 9, 924–935
© Materials Research Society, 2019
doi:10.1557/mrc.2019.115

MRS Communications

Prospective Article

# A perspective on triplet fusion upconversion: triplet sensitizers beyond quantum dots

**Zachary A. VanOrman†, Alexander S. Bieber†, Sarah Wieghold,** and **Lea Nienhaus**, Department of Chemistry and Biochemistry, Florida State University, 95 Chieftan Way, Tallahassee, FL 32306, USA

Address all correspondence to Lea Nienhaus at **lnienhaus@fsu.edu**

(Received 3 July 2019; accepted 7 August 2019)

## Abstract

The processes of singlet fission and triplet fusion could allow state-of-the-art photovoltaic devices to surpass the Shockley–Queisser limit by optimizing the utilized solar spectrum by reducing thermal relaxation and inaccessible sub-bandgap photons, respectively. Triplet fusion demands precise control of the spin-triplet state population, and requires a sensitizer to efficiently populate the triplet state of an acceptor molecule. In this perspective, we highlight the established field of sensitized upconversion and further examine alternative triplet sensitization routes, including the possibility of bulk solid-state semiconductors as triplet sensitizers, which provide a new avenue for charge transfer-based triplet sensitization rather than excitonic triplet energy transfer.

## Introduction

Efficient control and generation of spin-triplet states are essential for the understanding and advancement of current technologies, especially in regard to applications in photovoltaic (PV) devices. The processes of singlet fission (SF) and triplet fusion, or triplet–triplet annihilation upconversion (TTA-UC) depend on spin-triplet states to interconvert the wavelengths of the incident light and the resulting emission. The SF process involves the splitting of a higher-lying singlet state into two triplet states that can be harvested as photocurrent in PV devices,[1–5] whereas the opposite process of TTA-UC combines two triplet states to a higher-lying singlet state in a spin-allowed process that results in upconverted emission upon relaxation of the resultant singlet state.[6–8] TTA is commonly observed in heavily conjugated organic molecules, such as polyacenes. Here, the electronic interactions between two triplet states on adjacent molecules allow for "annihilation" to a single higher lying singlet state.

In general, UC as a result of TTA has wide-ranging applications which include overcoming the Shockley–Queisser limit in single-junction solar cells,[9,10] photocatalysis,[11–14] three-dimensional displays,[15] bioimaging,[16] and sub-bandgap sensitization of silicon-based devices for infrared (IR) imaging.[17] However, as transitions from the singlet ground state to excited spin-triplet states are "spin-forbidden," the triplet state must be indirectly populated, or sensitized, in order to efficiently harness their energy. This sensitization process can occur through a spin-allowed Dexter triplet energy transfer (TET) mechanism,[18] where the triplet state of the acceptor molecule can be populated by a direct excitonic energy transfer from the sensitizer or through charge transfer of independent carriers to the bound triplet state.[19–21] For the past years, metal–organic complexes with high spin–orbit coupling constants have commonly been used, which allow for the generation of triplet states through intersystem crossing (ISC).[6] However, large energy losses due to exchange energies up to 300 meV can still occur during the ISC process and limit the overall energy gained by the UC process.[6,22] To overcome this limitation in the achievable UC efficiency, semiconducting nanocrystals (NCs) have been explored as sensitizers. NCs have several advantages over the previous metal–organic complexes: (i) strong spin–orbit coupling results in their unique wavefunction which exhibits both singlet and triplet character and (ii) small exchange energies, resulting in minimal energy losses in the triplet sensitization process.[23–25] In addition, NCs are prime candidates to be used as sensitizer materials in TTA-UC systems[26–28] due to their facile synthetic bandgap tunability as well as exceptional photophysical properties.[29] However, bulky surface ligands are required for both colloidal stability and surface passivation of NCs and can limit the UC efficiency,[30] as they pose an additional tunneling barrier for TET.[18,30–33] When incorporated into solid-state devices, the performance of NC-based UC devices has also been low due to low optical absorbance based on film thickness limitations. These limitations mostly result from inefficient exciton diffusion,[34] making application and compatibility of UC devices to state-of-the-art PV devices still relatively far away.[34] In this perspective, we briefly introduce TTA-UC, followed by a review of materials used in state-of-the-art UC devices. In the last section of this perspective, we discuss new approaches to

† These authors contributed equally to this work.


https://doi.org/10.1557/mrc.2019.115 Published online by Cambridge University Press

triplet sensitization that expands beyond semiconductor NCs, such as bulk perovskite sensitization of rubrene triplet states through a charge transfer process.

## Threshold intensity for efficient upconversion

The goal is to implement TTA-UC in state-of-the-art PV devices requiring the UC process to be efficient at solar, or even sub-solar fluxes. In general, the UC efficiency, denoted as $\eta_{UC}$, is defined as the percentage of low energy photons absorbed that contribute to UC, and result in higher-energy emissive states in the acceptor molecule.[6,11] $\eta_{UC}$ can be obtained from the product of the energy transfer efficiency ($\eta_{ET}$) from the sensitizer to the annihilator, the TTA efficiency of the annihilator ($\eta_{TTA}$), and the photoluminescence quantum yield (PLQY) of the annihilator/emitter ($\eta_{ann}$).[35]

$$\eta_{UC} = \eta_{ET} \cdot \eta_{TTA} \cdot \eta_{ann}. \quad (1)$$

The UC efficiency $\eta_{UC}$ is power dependent and a commonly accepted method of determining the efficiency threshold of TTA resulting in singlet states relies on the power dependence of the UC PL. In a log–log plot of PL intensity versus laser excitation density, the intensity threshold $I_{th}$ at which TTA becomes efficient can be observed (Fig. 1).[36–38] In the region where TTA is inefficient, a quadratic power dependence is observed: slope of $\alpha = 2$. The quadratic region denotes a quasi-first order triplet recombination pathway involving phosphorescence, quenching, and nonradiative relaxation to the ground state. Above the threshold $I_{th}$, a linear dependence can be observed (slope $\alpha = 1$), which results from the recombination of the triplet population primarily through the desired TTA pathway creating high-energy singlets.[36–38]

## Metal–organic complexes as triplet sensitizers

For the past decade, metal–organic complexes have been widely studied as sensitizers in TTA-UC systems.[6] The heavy metals in these complexes, e.g., Pt,[39,40] Pd,[41,42] or Ru[43,44] enhance spin–orbit coupling, thereby mediating efficient ISC to the triplet excited state. In a metal–organic-sensitized system, the metal–organic complex sensitizer is excited from its ground state to an excited singlet state followed by ISC to a triplet state. TET to the acceptor molecule populates the triplet state of the acceptor enabling TTA-UC.

Although "delayed fluorescence" as a result of TTA was first discovered by C.A. Parker in 1962,[45] metal–organic-sensitized TTA was not observed until much later. In one of the first reports of metal–organic-sensitized TTA in 2004,[43] the following complex was used: $[Ru(dmb)_2(bpy\text{-}An)]^{2+}$, where dmb is 4,4′-dimethyl -2,2′-bipyridine and bpy-An is 4-methyl-4′-(9-anthrylethyl)-2,2′-bipyridine. UC emission resulted *via* metal–organic-sensitized TTA upon 450 nm excitation. The excitation of the system produces a metal-to-ligand charge transfer (MLCT) triplet state that can efficiently sensitize the anthracene triplet state, resulting in TTA-UC. This sensitization scheme relies on the alignment of energy levels, as the triplet energy level of anthracene is lower than the triplet MLCT excited state, but the singlet excited state of anthracene is higher in energy than the singlet MLCT excited state.[46]

Subsequent reports of green-to-blue UC by Castellano and co-workers[44] using 9,10-diphenylanthracene (DPA) as a triplet acceptor in the place of anthracene resulted in a significant increase in the intensity of the observed UC emission, which also allowed for lower incident excitation powers.[44] This was attributed partly to the increased QY of DPA as compared to anthracene ($\Phi = 0.95$ and 0.27, respectively)[47] but also due to the decreased likelihood of dimerization in DPA as compared to anthracene.

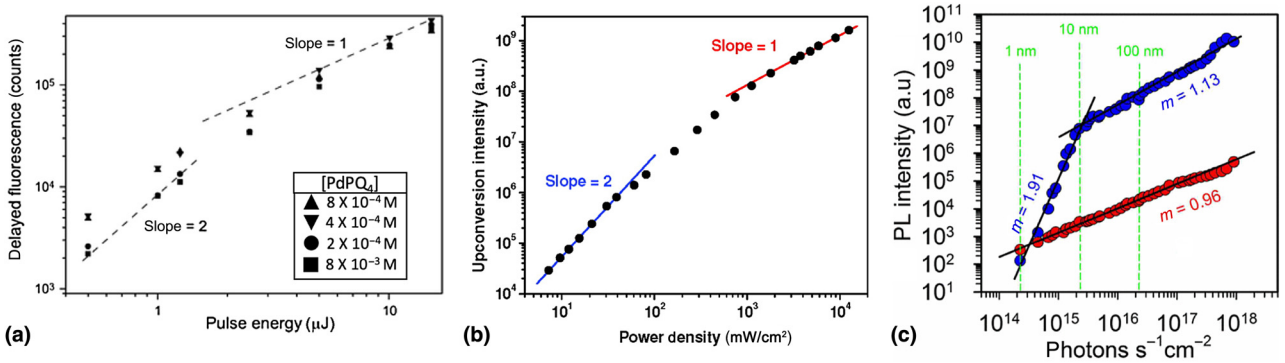



**Figure 1.** (a) The PL power dependency of different sensitizer concentrations of a solution-based palladium(II)tetrakisquinoxalinoporphyrin ($PQ_4Pd$)/rubrene upconversion system where both maximized performance is observed above the intensity threshold (linear dependence, slope = 1), as well as a quadratic dependency (slope = 2) below the threshold intensity $I_{th}$. Adapted from Ref. [36] with permission from the PCCP Owner Societies. (b) PL power dependence of a palladium(II)octaethylporphyrin (PdOEP)/DPA mixture. Adapted from Ref. [37] with permission. Copyright 2012 The American Chemical Society. https://doi.org/10.1021/jz300012u. Further permissions related to the material excerpted should be directed to the ACS. (c) PL power dependency of a platinum(II)octaethylporphyrin (PtOEP)/DPA mixture. The upconverted emission is shown as blue circles where the phosphorescent emission from PtOEP is shown as red circles. Adapted with permission from Ref. [38]. Copyright 2008 American Physical Society.



https://doi.org/10.1557/mrc.2019.115 Published online by Cambridge University Press

Singh-Rachford et al.[39,40] achieved red-to-blue TTA-UC using platinum(II) tetraphenyltetrabenzoprophyrin (PtTPBP) as their sensitizer. An energy gain of 0.80 eV in the UC process was observed when coupled with the acceptor molecule perylene, a polycyclic aromatic hydrocarbon.[40] The UC efficiency was determined to be only $0.00065 \pm 0.0001\%$ for this system. This low efficiency was suggested to be from competing nonradiative pathways such as electron transfer quenching or perylene excimer formation.[40]

However, many challenges still exist for metal–organic sensitizers. Some key limitations include large energy losses in ISC, low relative photostability, and the difficulty to efficiently operate beyond the near-infrared (NIR) region.[26] In particular, the energy gap law[48] predicts an increase in the nonradiative recombination rate for decreasing energy of the $S_0$–$S_1$ transition.[49] For UC to add efficiency to PV devices, it is crucial to upconvert IR light below the bandgap of silicon.[50]

Another challenge for metal–organic sensitizers is the UC of visible-to-ultraviolet (UV) light. Currently, there have only been a limited number of reports of efficient visible-to-UV UC by Castellano and others.[51–55] One detrimental issue is the parasitic reabsorption of the UC emission. Since the UC emission is within the absorption of the sensitizer, there is also singlet–singlet energy back-transfer.[51] This greatly hinders the UC QY and thus results in very high excitation powers required for efficient TTA.

## Quantum dot sensitization

Another class of material is semiconductor NCs or quantum dots (QDs), which present an alternative sensitization route that offers several advantages over metal–organic systems. Strong spin–orbit coupling in these NCs mixes wavefunctions with singlet and triplet character, allowing for efficient coupling of the exciton to a molecular triplet state. Facile synthetic and compositional bandgap tuning enables NCs to function as sensitizers over a large spectral range spanning the visible and short-wave IR allowing for the selection of a UC wavelength far beyond 800 nm.[26] Commonly used NCs for sensitization of TTA-UC systems are based on either cadmium or lead chalcogenides, including CdSe,[56–58] PbSe,[26] and PbS.[32,59–61]

The triplet character of the wavefunction of semiconductor NCs was initially shown to be able to create singlet oxygen ($^1O_2$) by TET, which is a competing pathway to the TTA-UC desired here.[58,62,63] The use of NCs in photon interconversion applications was first discovered by the reverse process of SF in 2014,[64,65] but it was reported soon after that, that such semiconductor NCs can also function as efficient sensitizers for TTA-UC applications.[26–28,35,58,66,67] Figures 2(a) and 2(b) detail the process of TTA-UC in the two different systems, namely metal–organic and NC sensitization, respectively.[27] Figure 2(a) shows the basic mechanism for TTA-UC utilizing metal–organic sensitization as discussed in the previous section: the initially excited singlet exciton undergoes ISC to the triplet state $T_1$. This triplet state is then transferred to the annihilator *via* triplet–triplet energy transfer (TTET). Electronic interactions of two adjacent triplet states can result in TTA, creating the higher energy emissive singlet state. In NC-sensitized UC [Fig. 2(b)] on the other hand, the loss due to the exchange energy can be reduced as their strong spin–orbit coupling results in wavefunctions exhibiting both singlet and triplet character.[23] The optically excited exciton in the NC is transferred directly to the triplet state of the annihilator, and TTA results in the generation of an emissive high-energy singlet state.

Although this alternative route of employing semiconducting NCs as sensitizers in TTA-UC systems readily showed an improved UC efficiency over metal–organic complexes, there is still a need to further improve the systems QY. Here, a path towards improving the efficiency of NC semiconductor-sensitized systems involves the use of core–shell NCs, where the surface of the NC is passivated by a shell composed of a wider bandgap material [Fig. 2(c)].[27] The shell reduces defect sites where nonradiative recombination can occur hence, the photophysical properties are greatly improved. However, as shown in Figs. 2(c) and 2(d), the addition of a shell presents another problem: an additional tunneling barrier hindering efficient TET.[68] As can be seen, the UC QY increases initially when creating a passivating shell but then sharply decreases with increasing shell thickness since Dexter transfer is exponentially dependent on the donor–acceptor spacing.[18] This indicates that shells must be kept thick enough to limit nonradiative recombination on the NC surface but thin enough to enable efficient TET to the transmitter ligand or acceptor molecule. In Fig. 2(c), for a PbS QD core with a CdS shell, this interplay between the thickness of the shell and UC QY is shown. In the first regime between a CdS shell thickness of 0 and 0.1 nm, the UC QY increases to a maximum. Beyond that point, the UC QY decreases as a function of the shell thickness. However, the thickness of the shell alone is not the only factor relevant to the UC QY. As shown in Fig. 2(d), the size of the QD core also has an impact on the UC QY, as a smaller core QD requires a larger shell to passivate an increased number of surface traps relative to its size.[69] Nevertheless, the same trend as in Fig. 2(c) is still observed for all core diameters.

However, one significant challenge remains, which limits the UC efficiency of these NC-sensitized TTA systems. Semiconductor NCs rely on bulky ligands required to passivate their surface and for colloidal stability. These ligands can significantly limit the TET efficiency between sensitizer and acceptor, due to the exponential distance dependence of the Dexter energy transfer mechanism.[18] By implementing transmitter ligands, which funnel the triplet to the outer ligand shell, the TET efficiency can be greatly increased.[30,33] Strategy A (Fig. 3) details a PbSe NC sensitizer, which is simply mixed with the acceptor rubrene in solution. Here the exciton must overcome the tunneling barrier posed by the ligands prior to TET. Strategy B (Fig. 3), however, adds a transmitter ligand. In using CdSe as a sensitizer modified with a 9-anthracenecarboxylic acid (9-ACA) transmitter ligand and a DPA acceptor, DPA exhibits emission $\sim 10^3$ times higher than without the transmitter ligand.[30]


https://doi.org/10.1557/mrc.2019.115 Published online by Cambridge University Press

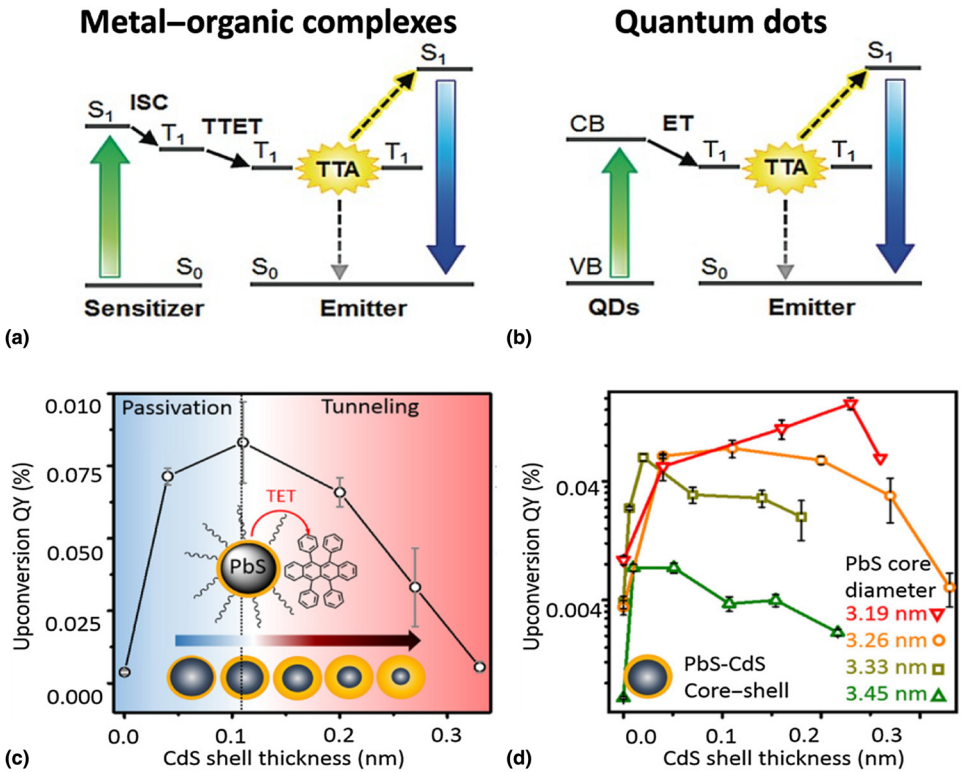



**Figure 2.** (a) Metal–organic-sensitized TTA-UC: intersystem crossing (ISC) from the singlet to the triplet state, followed by triplet–triplet energy transfer (TTET). Subsequent TTA of two triplets $T_1$ yields the higher-energy emissive singlet state. (b) Quantum dot-sensitized TTA-UC: energy transfer (ET) from the conduction band (CB) to the triplet state $T_1$. The collision of two triplet states leads to TTA and emission from a higher energy singlet state. Adapted with permission from Ref. [27]. Copyright 2016 John Wiley and Sons. (c) In a PbS core QD with a CdS shell, the UC QY when coupled with rubrene initially increases when the thickness of the CdS shell is increased. However, after reaching a maximum, the upconversion QY diminishes with increasing shell thickness, as the shell imposes an additional tunneling barrier. (d) Upconversion QY of four different PbS–CdS core–shell QD systems as a function of the CdS shell thickness and the PbS core dimension. Adapted with permission from Ref. [68]. Copyright 2016 American Chemical Society. https://doi.org/10.1021/acs.nanolett.6b03503. Further permissions related to the material excerpted should be directed to the ACS.

This approach is also implemented in work done by Okumura et al.[27] where a CdSe NC is modified with a ZnS shell prior to the addition of transmitter ligands. In this work, the $I_{th}$ value and the UC efficiency $\eta_{UC}$ were monitored for three systems: a core–shell NC, a core–shell NC modified with transmitter ligands, and a NC with no shell but modified with a transmitter ligand. The addition of transmitter ligands to the core–shell NC increased both the $I_{th}$ and $\eta_{UC}$ largely,

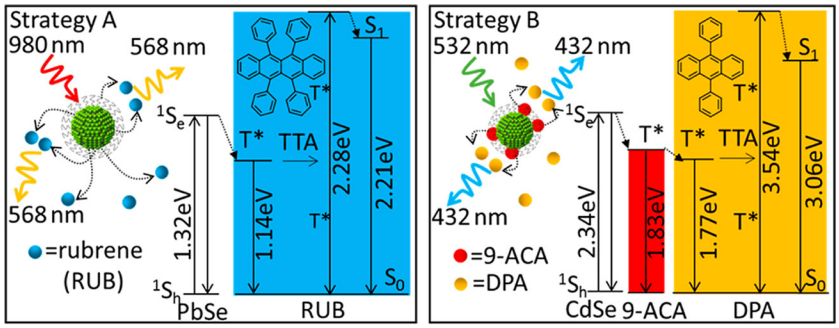



**Figure 3.** Schematic detailing two approaches toward QD sensitization. Strategy A is the direct sensitization of the acceptor triplet state ($T^*$), whereas strategy B uses sensitization of a transmitter ligand (9-ACA) that consequently performs triplet energy transfer to the acceptor. Reproduced from Ref. [33] with permission. Copyright 2015 American Chemical Society. https://doi.org/10.1021/acs.nanolett.5b02130. Further permissions related to the material excerpted should be directed to the ACS.



https://doi.org/10.1557/mrc.2019.115 Published online by Cambridge University Press

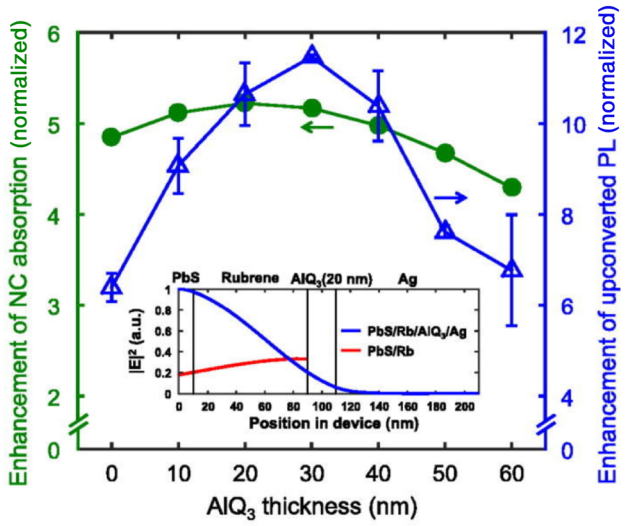



**Figure 4.** The effect of $AlQ_3$ thickness on the absorption of the NC layer and the UCPL. The NC layer absorption enhancement (green) decreases upon the increase of the thickness $AlQ_3$ layer, while the UCPL is enhanced from the up to a thickness of the $AlQ_3$ layer of 30 nm after which it then decreases. Adapted from Ref. [70] with the permission of AIP Publishing.

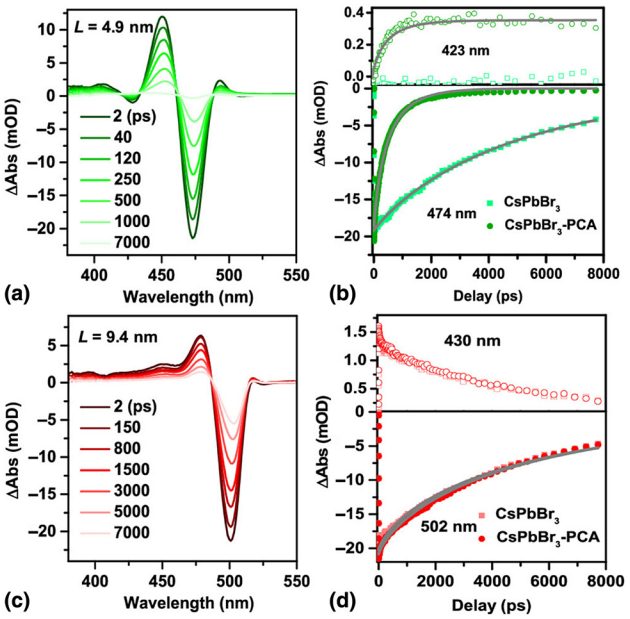



**Figure 6.** (a) Transient absorption (TA) spectra of a $CsPbBr_3$–PCA complex with an edge length of $L = 4.9$ nm at different delay times, $\lambda_{ex} = 470$ nm. (b) TA kinetics at 423 nm (top, open symbols, PCA triplet absorption) and 474 nm (bottom, solid symbols, $CsPbBr_3$ exciton bleach) for $CsPbBr_3$ and the $CsPbBr_3$–PCA complex with $L = 4.9$ nm. The solid lines correspond to stretched exponential fits for each decay trace. (c) TA spectra of the $CsPbBr_3$ NC-PCA system with an edge length of $L = 9.4$ nm, $\lambda_{ex} = 470$ nm. (d) TA kinetics at 430 nm (top, open symbols) and 502 nm for $CsPbBr_3$ and $CsPbBr_3$–PCA complex with $L = 9.4$ nm. Reproduced from Ref. [71] with permission. Copyright 2019 American Chemical Society. https://doi.org/10.1021/jacs.8b13180. Further permissions related to the material excerpted should be directed to the ACS.

but the core–shell NC also outperformed the NC with no shell modified with transmitter ligand, highlighting the role of NC surface defects on both the $I_{th}$ and the overall efficiency of UC.

Following these reports of solution-based NC-sensitized UC, semiconductor NCs have also been integrated into solid-state devices. Devices are fabricated by spin-casting PbS NCs onto a substrate followed by thermal evaporation of rubrene/0.5% tetraphenyldibenzoperiflanthene (DBP) in a guest–host/annihilator–emitter pair.[28,32,70] Reports by Baldo and co-workers show that the UC efficiency of the device can be further increased by the addition of a reflective layer as well as a dielectric spacer, as this device structure effectively increases the absorption of the NC film through interference effects that enhance the optical field.[70] The UC emission obtained from the device is increased by up to an order of magnitude by the addition of an $AlQ_3$ spacer layer and Ag reflective layer and is dependent on the thickness of the $AlQ_3$ layer (Fig. 4). The combination of this interference enhancement and a reduction in the NC–rubrene spacing by ligand exchange

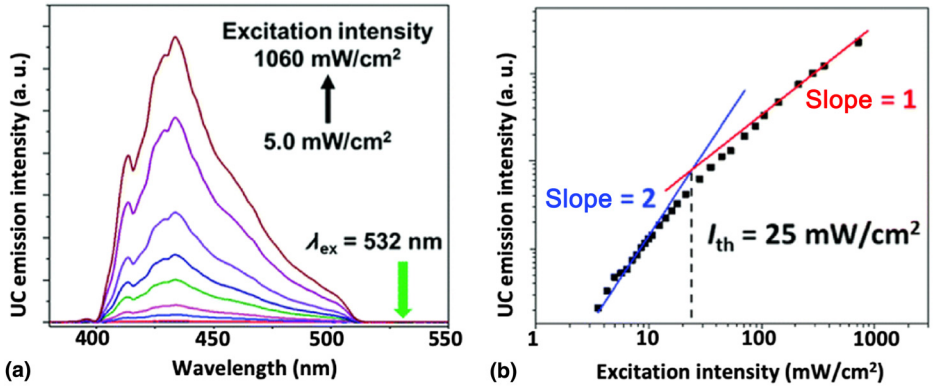



**Figure 5.** (a) UC PL monitored at 532 nm different excitation intensities. (b) Power dependence of the UC emission intensity at 430 nm. The $I_{th}$, 25 mW/cm$^2$, is found at the intersection between the lines of slope = 2 and slope = 1. Reproduced from Ref. [67] with permission from The Royal Society of Chemistry.


https://doi.org/10.1557/mrc.2019.115 Published online by Cambridge University Press

consequently yielded a current solid-state PbS NC-sensitized UC efficiency of 7%.[32]

A kinetic model based on the aforementioned PbS solid-state UC system was developed to recreate the PL dynamics in both a monolayer and multilayered sensitized UC system.[34] Interestingly, the addition of another PbS monolayer to the PbS/rubrene system has little effect on the intensity of the UC PL due to inefficient exciton transport through the PbS film. The addition of the second monolayer of PbS NCs introduces pathways that are disruptive to the UC efficiency: long-range Förster-like energy transfer from rubrene to the distant PbS film. The model highlights that parasitic back-transfer from rubrene to PbS is problematic even in single monolayer devices and may lead to the large discrepancy between the near-unity TET and the 7% $\eta_{UC}$ reported previously.[32]

## Beyond conventional quantum dots—excitonic perovskites

Following the reports of conventional semiconductor NCs as triplet sensitizers, perovskite NCs have also been explored as potential triplet sensitizers.[67,71,72] In 2017, Mase et al.[67] performed the first UC experiment utilizing perovskite NCs for triplet sensitization in TTA-UC applications. They used $CsPbX_3$ nanocrystals ($X$ = Br, **I**), DPA as the acceptor, and a DPA derivative as the transmitter ligand. As shown by Fig. 5(a), the UC emission was observed at ~430 nm under 532 nm excitation. The $I_{th}$ value [Fig. 5(b)] was obtained by measuring the power dependence of the UC emission intensity, resulting in $I_{th} = 25$ mW/cm$^2$, demonstrating that perovskite NCs efficiently sensitize DPA triplets under low illumination densities. The UC efficiency was estimated at 1.3%.

To further explore the potential of perovskite NCs as triplet sensitizers, the dynamics of TET from the perovskite NCs to 1-pyrenecarboxylic acid (PCA), a triplet acceptor, were investigated by transient absorption (TA) spectroscopy, as shown in Fig. 6.[71] TA spectra of $CsPbBr_3$ and the corresponding $CsPbBr_3$–PCA complex are shown in Fig. 6(a) for a NC with an edge length of $L = 4.9$ nm. The TA kinetics were selectively probed at two wavelengths, one attributed to exciton bleaching [474 nm in Fig. 6(b)] and the other to the $T_1 \rightarrow T_n$ transition [423 nm in Fig. 6(b)] in the NC-PCA systems. As shown in Fig. 6(b), the lifetime of the exciton bleach is quenched upon addition of triplet acceptor. In contrast, the larger NCs ($L = 9.4$ nm) shown in Figs. 6(c) and 6(d) show no indication of additional quenching upon the addition of PCA, and the $T_1 \rightarrow T_n$ transition in PCA is not observed, leading the authors to conclude that quantum confinement is required for TET to occur in this system.

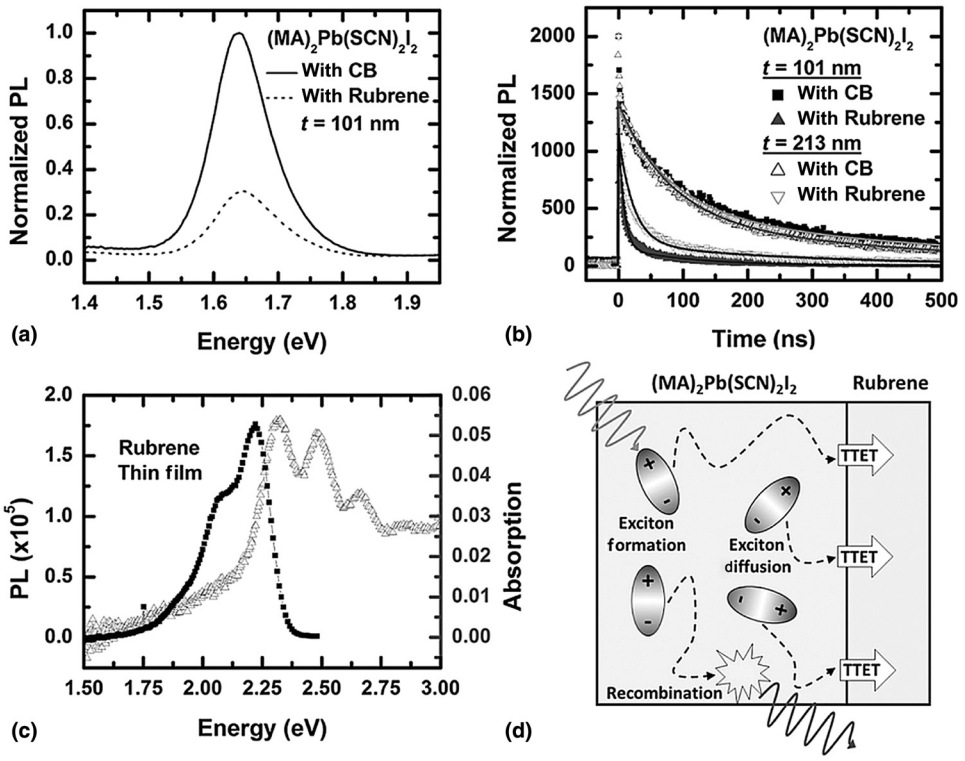



**Figure 7.** (a) Steady-state PL of 2D $(MA)_2Pb(SCN)_2I_2$ with chlorobenzene (solid line) and with rubrene solution-cast from chlorobenzene (dotted line) added. (b) Time-resolved PL of $(MA)_2Pb(SCN)_2I_2$ with chlorobenzene (dark squares for 101 nm film, open triangle for 213 nm film) and with rubrene (filled triangle for 101 nm film and upside-down open triangle for 213 nm film). (c) Absorption spectrum (gray) and steady-state PL (black) of rubrene under 485 nm excitation. (d) Schematic of triplet exciton diffusion across the perovskite film, leading to TTET at the interface of the perovskite/rubrene layers. Reproduced from Ref. [73] with permission. Copyright 2016 John Wiley and Sons.



https://doi.org/10.1557/mrc.2019.115 Published online by Cambridge University Press

Excitonic TET to organic triplet acceptors has also been observed in a 2D perovskite thin-film material: $(CH_3NH_3)_2Pb(SCN)_2I_2$, which exhibits strong PL from the triplet state.[73] Figure 7(a) depicts the steady-state PL for the two investigated systems: $(CH_3NH_3)_2Pb(SCN)_2I_2$ in the absence and presence of rubrene. PL quenching in the presence of rubrene, a common triplet acceptor,[19,20,41,60] was observed both in steady-state [Fig. 7(a)] and time-resolved measurements [Fig. 7(b)], indicating TTET from the perovskite to rubrene. A comparison of the quenching behavior [Fig. 7(b)] for two different perovskite film thicknesses, i.e., 101 and 213 nm, indicates an increased quenching for the thinner film. This led to the conclusion that the long-lived triplet excitons created in the perovskite film diffuse to the interface and then can efficiently transfer to the triplet acceptor (e.g., rubrene, perylene).

## Beyond bound excitons—perovskite thin films

To overcome the limitations of NC-based devices, which as discussed previously, have been hindered in their advancement due to short exciton diffusion lengths, slow TET, and strong singlet reabsorption due to their broadband absorption, we investigate bulk materials as sensitizers. In the following, we will build on the previous paragraph of 2D perovskites and

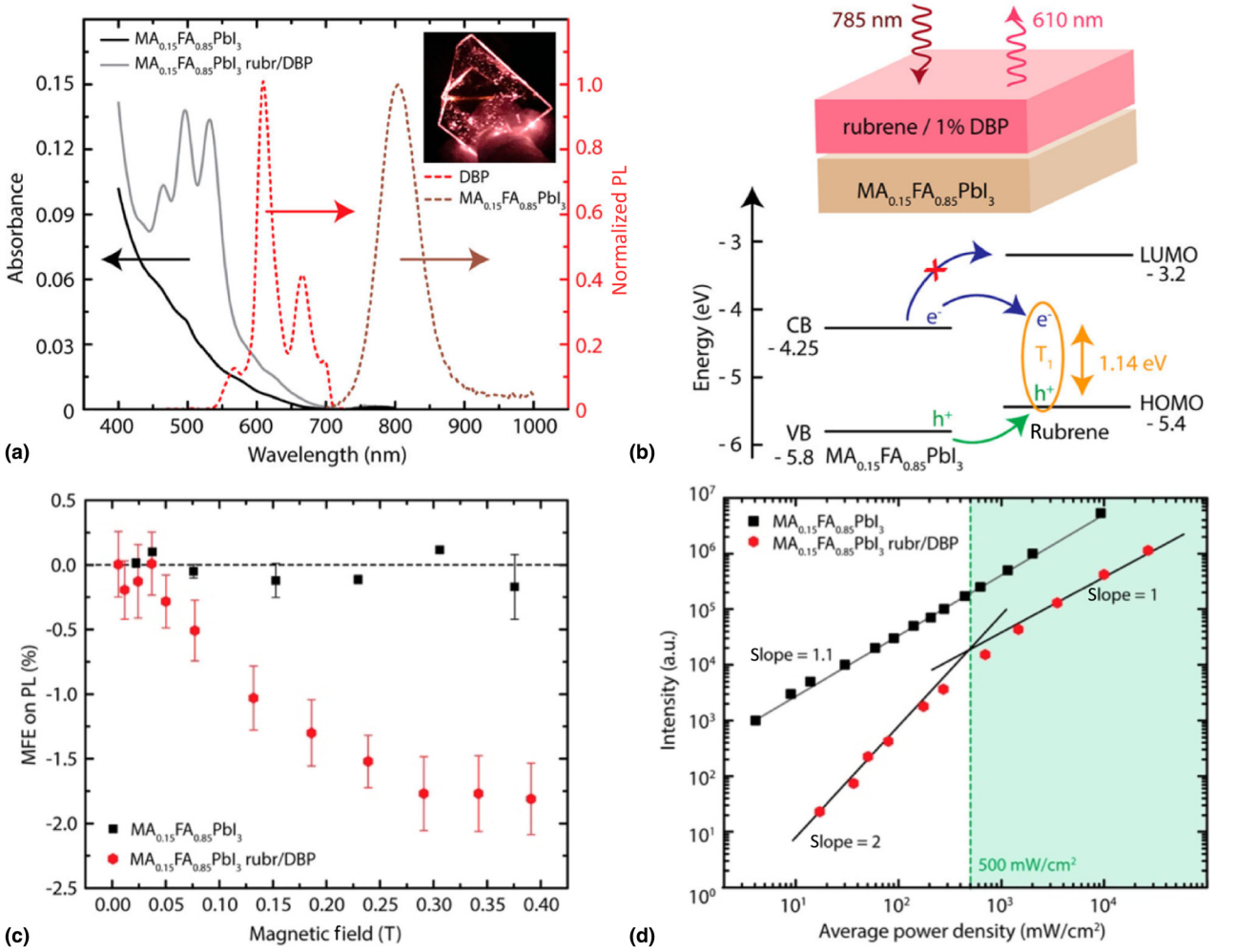



**Figure 8.** (a) Normalized absorption spectrum of the perovskite thin film (black) and the bilayer upconversion device (gray), consisting of the perovskite layer and a rubrene layer doped with 1% DBP, as well as steady-state PL of perovskite film emission (brown dotted line) and upconverted emission from the DBP (red dotted line). UC emission can be seen as an orange line when the device is exposed to a 785 nm laser, displayed in the figure inset. (b) UC device schematic, where, when under 785 nm excitation, emission at 610 nm from the DBP excited state occurs. Band energy diagram showing charge transfer from the perovskite to rubrene. The triplet state of rubrene is populated via hole extraction from the valence band (VB) of the perovskite, while the electron is extracted from the conduction band (CB) of the perovskite to the triplet state $T_1$ of rubrene. The mismatch in energy blocks direct injection of the electron to the LUMO of rubrene. (c) Magnetic field effect (MFE) on perovskite emission (black) and upconverted emission (red). (d) Power dependence of the perovskite emission (black) and the upconverted emission (red). The slope intersection denotes the $I_{th}$ of 500 mW/cm$^2$. Adapted with permission from Ref. [19]. Copyright 2019 American Chemical Society. https://doi.org/10.1021/acsenergylett.9b00283. Further permissions related to the material excerpted should be directed to the ACS.


https://doi.org/10.1557/mrc.2019.115 Published online by Cambridge University Press

investigate the triplet sensitization by bulk perovskite-based materials. Perovskite and perovskite-inspired materials are currently heavily studied for use in PV applications. In these bulk perovskite materials such as methylammonium lead triiodide ($MAPbI_3$) bulk films, bound excitons generally rapidly dissociate into free unbound free-charge carriers due to low exciton binding energies. In addition, high charge carrier diffusion lengths, long charge carrier lifetimes,[74–76] low nonradiative recombination,[77] and high absorbance in the visible and near IR make them promising for use as sensitizers in TTA-UC. While low exciton binding energies (on the order of kT) are favorable for PV applications, they offer uncharted waters in TTA-UC, as a triplet sensitization mechanism based on charge transfer must account for both the electron and hole injection from the sensitizer into the bound triplet state of the organic acceptor molecule. In contrast to a Dexter-type bound TET mechanism, the absolute energy levels of the sensitizer conduction band (CB) and valence band (VB) must be aligned with the triplet state of the annihilator. This geometry allows for energetically favored electron and hole transfer, without allowing for direct injection of the excited electron into the lowest unoccupied molecular orbital (LUMO) of the organic acceptor.[19]

Bulk 3D-perovskite materials were first integrated into solid-state TTA-UC systems by Nienhaus et al.[78] to serve as a NIR-absorbing antenna to increase the absorbance of a solid-state PbS NC/rubrene system. Although the absorbance increased, the UC efficiency was not notably enhanced because of a competing pathway: singlet back-transfer to the perovskite reduced the visible light output of the device. Based on this report, a new UC system was designed by directly using the bulk perovskite as the sensitizer.[19] A mixed cation lead iodide perovskite consisting of MA and formamidinium (FA) (MAFA) with a thickness of 14 nm is used as the sensitizer coupled to the annihilator/emitter rubrene doped with 1% DBP. Figure 8(a) highlights the optical absorption and emission properties of the bare perovskite film and the UC bilayer device in which the UC PL under 785 nm excitation is seen at ~610 nm (compare inset). The device structure is highlighted in the schematic in Fig. 8(b) on the top: MAFA is first spin-coated onto a glass substrate followed by a layer of solution-cast rubrene/DBP. The device absorbs incident 780 nm photons and subsequently emits at ~610 nm. The band diagram [Fig. 8(b), bottom] indicates that the energy band alignment is favorable for triplet sensitization by charge injection while disallowing direct electron injection into the LUMO of rubrene.

In order to ensure the visible light obtained from the UC device is indeed due to TTA and not due to a different mechanism, the magnetic field effect (MFE) was measured for the bare MAFA perovskite thin film and the UC bilayer device consisting of MAFA + rubrene/DBP. Figure 8(c) shows the change in the UC PL and MAFA PL as a function of the applied magnetic field confirming the typical nonmonotonic negative MFE signature of TTA.[79]

To further support a TTA-based UC mechanism in the MAFA/rubrene system, the power dependency of the UC PL was examined. Figure 8(d) shows the PL intensity as a function of the incident average power density where the expected slope change from $\alpha = 2$ to $\alpha = 1$ is observed, further confirming the hypothesis of TTA. This slope change occurs at $I_{th} = 500$ mW/cm$^2$, which is ~20-fold lower than the lowest $I_{th}$ reported for a comparable device comprised of PbS NCs.[28] However, due to the low NIR absorption of the 14 nm thin MAFA layer, only the external quantum efficiency of the UC process can accurately be determined at $(1.5 \pm 0.3) \times 10^{-4}$ %. A conservative estimate of the internal UC efficiency yields $\eta_{UC} = 3.1\%$.[19]

To boost the absorption of the perovskite thin film and also investigate the role of trap states on the UC process, the MAFA film thickness was modified.[20] Several main observations were made: (i) trap filling and charge transfer to rubrene compete [Fig. 9(a)]. (ii) The increased quality of thicker MAFA films resulting from larger grains and reduced trap sites translates into longer carrier lifetimes, which enables a more efficient charge transfer process and results in "sub-solar" $I_{th}$

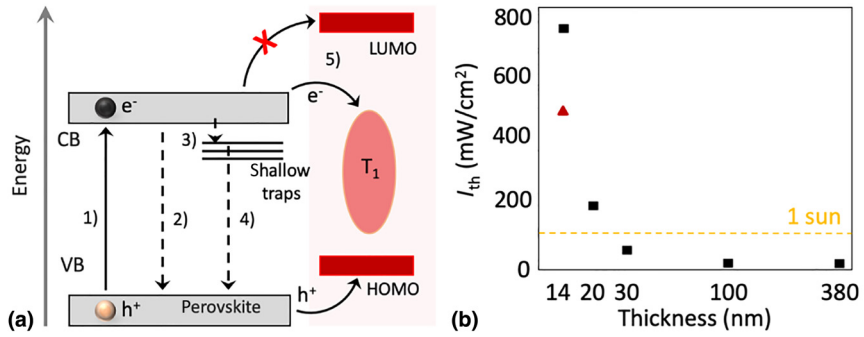



**Figure 9.** (a) Processes occurring in the UC bilayer device upon excitation at 780 nm. (1) An electron is excited from the valence band to the conduction band in the perovskite film. This electron can be quenched by multiple possible pathways: (2) bimolecular free carrier recombination, (3) shallow trap filling, (4) monomolecular trap-assisted recombination, or (5) charge transfer to rubrene. Adapted from Ref. [20] Copyright 2019 with permission from Elsevier. (b) The $I_{th}$ of the MAFA/rub. devices as a function of their thicknesses. The device from Ref. [19] is denoted by the red triangle, as it was measured with a pulsed excitation source. All others measured using continuous wave (CW) excitation.



https://doi.org/10.1557/mrc.2019.115 Published online by Cambridge University Press

values at thicknesses above 30 nm [Fig. 9(b)]. (iii) The expected slope change of $\alpha = 2$ to $\alpha = 1$ at the threshold intensity $I_{th}$[36–38] shifts to follow the power-law dependence of the MAFA PL: $I_{UCPL} \sim F^{\beta} = (I_{MAFA})^2 = F^{2\alpha}$.[20] However, parasitic back-transfer of created singlets limits how thick the perovskite layer can be; despite a decrease in the $I_{th}$ value for the thickest MAFA film investigated (~380 nm), the visible light output was barely increased over the 100 nm thick film. This indicates there is a tradeoff in the absorption of the film and the visible light output of the UC device.[20]

In addition, two unexpected results have been reported in these MAFA + rubrene bilayer devices: (i) the occurrence of two rising components in the UC PL, as well as (ii) a photodarkening of the UC PL obtained from the device. To find the root cause of these effects, the role of triplet diffusion on perovskite-sensitized TTA in rubrene was investigated.[21]

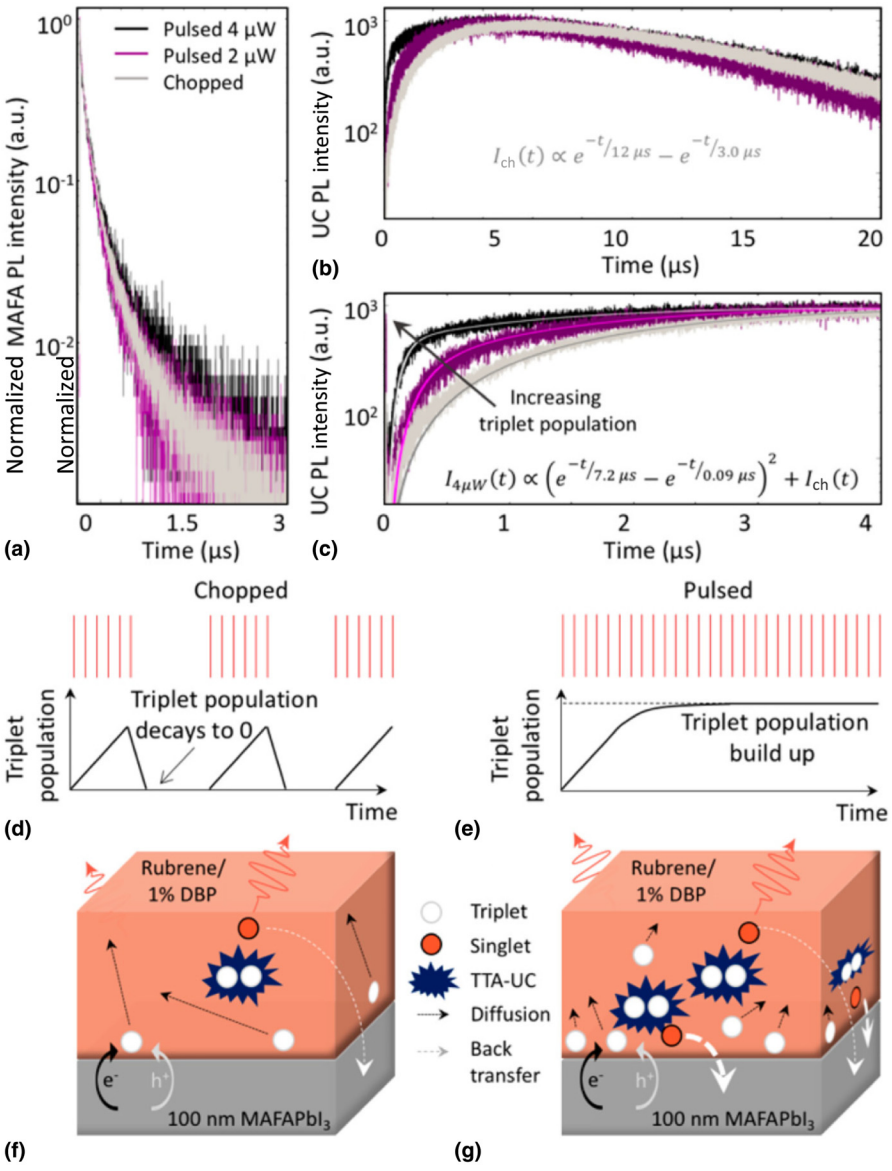



**Figure 10.** (a) MAFA PL lifetimes (>800 nm) as a result of incident power (4 μW in black, 2 μW in purple) as well as the addition of a chopper wheel (gray). (b) UC PL lifetimes (560–640 nm) monitored in the same manner as the MAFA PL lifetimes. (c) A zoomed-in view of (b), detailing the different rise times shown under the three measurement conditions. (d) A schematic showing the effect of a chopper with a 25 ms "off time" (time in between pulse) on the triplet population. (e) A schematic showing the triplet population increasing without decay with no "off time" from the laser. (f) Schematic detailing TTA as a result of slow triplet diffusion, where the triplet states have longer diffusion lengths due to relatively low triplet concentrations in the annihilator. (g) Schematic detailing TTA as a result of smaller triplet diffusion lengths and a larger concentration of triplet states. Back transfer of singlet states is more prevalent due to TTA occurring close to the sensitizer. Reprinted with permission from Ref. [21]. Copyright 2019 American Chemical Society. https://doi.org/10.1021/acs.jpclett.9b01526. Further permissions related to the material excerpted should be directed to the ACS.


https://doi.org/10.1557/mrc.2019.115 Published online by Cambridge University Press

In diffusion-mediated TTA, triplets diffuse until finding another triplet state to annihilate with. The effective diffusion length of the triplet states in the annihilator will be dependent on the triplet population, as a higher triplet density will result in more frequent collisions. To modulate the triplet population, a 20 Hz mechanical chopper was introduced to allow the triplet population and potential long-lived trapped charge carriers in the perovskite sensitizer to fully relax. To discern whether the effects observed were caused by the MAFA sensitizer [Fig. 10(a)] or the rubrene/DBP annihilator/emitter pair [Figs. 10(b) and 10(c)], the PL dynamics were monitored under pulsed conditions (black), pulsed modulated conditions (gray), and pulsed conditions at half the average power (purple). As the MAFA PL decay does not show condition-dependent dynamics, the rubrene must be responsible for the unusual effects observed. As shown in Fig. 10(b) and in other perovskite-sensitized TTA systems,[19,20] the UC PL under standard pulsed conditions (black) has three distinct regions: (1) a fast rise in the first few hundred nanoseconds, (2) a slower rise until ~5 μs, and (3) a gradual decay beyond 5 μs.

Clearly visible is a power dependence of the UC PL dynamics: the ratio of the fast and slow rises varies. Here, we refer to the schematics in Figs. 10(d) and 10(e), highlighting how the triplet population depends on the type of excitation. As established previously, the triplet diffusion length is dependent on the triplet population. With this fact, the underlying cause of the two rise times can be attributed to rapid TTA close to the interface due to a high triplet population (fast rise), while the slow rise stems from slow diffusion-mediated TTA far from the interface, compare Figs. 10(f) and 10(g).

The use of the mechanical chopper wheel was also found to increase the UC QY, as the triplets were allowed to diffuse far from the perovskite sensitizer layer before annihilating. In the case of low triplet diffusion, triplets annihilate near the sensitizer layer, which can lead to strong singlet back-transfer.

## Outlook

We have highlighted several approaches to triplet sensitization for TTA-UC ranging from metal–organic complexes, inorganic NCs, and bulk lead-halide perovskites. These results indicate that triplet sensitization by direct free-carrier injection is a promising and broadly applicable pathway to more efficient TTA-UC, enabling real-world applications of UC devices in PVs. In particular, other bulk materials that have proper band alignment to directly transfer carriers into triplet states should be investigated. In particular, it would be of interest if the spin–orbit coupling is required in this sensitization route, or if it is independent. Additionally, reports indicate that transition metal dichalcogenides such as $MoS_2$ can be utilized as triplet sensitizers, despite no current reports of using this avenue for TTA-UC.[80,81]

While the issue of low absorption of such UC devices has been able to be resolved by implementing bulk lead-halide perovskites with long free-carrier diffusion lengths as the triplet sensitizer, one major issue remains. Due to the overlap between the sensitizer absorbance and UC emission, the singlets created by UC are strongly far-field reabsorbed or back-transferred via efficient resonance energy transfer. There are several approaches possible to overcome this issue: (i) implementation of a triplet sensitizer with a defined absorption band that does not strongly overlap with the UC emission. (ii) A device structure which funnels the excitations away from the interface effectively, allowing for emission far from the strongly reabsorbing interface. We have previously shown that the triplet population level directly influences the UC emission obtained from the device, due to an increased rate of TTA close to the interface.

This indicates that further device optimization, in particular, tuning the relationship between the triplet sensitization rate and triplet diffusion rate, may be the key to unlocking the full potential of UC devices for applications in e.g., PVs.

## Acknowledgments

The authors gratefully acknowledge Florida State University startup funds.

## References

1 J. Lee, P. Jadhav, P.D. Reusswig, S.R. Yost, N.J. Thompson, D.N. Congreve, E. Hontz, T. Van Voorhis, and M.A. Baldo: Singlet exciton fission photovoltaics. *Acc. Chem. Res.* **46**, 1300 (2013).
2 M.B. Smith and J. Michl: Singlet fission. *Chem. Rev.* **110**, 6891 (2010).
3 M.C. Hanna and A.J. Nozik: Solar conversion efficiency of photovoltaic and photoelectrolysis cells with carrier multiplication absorbers. *J. Appl. Phys.* **100**, 074510 (2006).
4 D.N. Congreve, J. Lee, N.J. Thompson, E. Hontz, S.R. Yost, P.D. Reusswig, M.E. Bahlke, S. Reineke, T.V. Voorhis, and M.A. Baldo: External quantum efficiency above 100% in a singlet-exciton-fission–based organic photovoltaic cell. *Science* **340**, 334 (2013).
5 M. Einzinger, T. Wu, J.F. Kompalla, H.L. Smith, C.F. Perkinson, L. Nienhaus, S. Wieghold, D.N. Congreve, A. Kahn, M.G. Bawendi, and M. A. Baldo: Sensitization of silicon by singlet exciton fission in tetracene. *Nature* **571**, 90 (2019).
6 T.N. Singh-Rachford and F.N. Castellano: Photon upconversion based on sensitized triplet–triplet annihilation. *Coord. Chem. Rev.* **254**, 2560 (2010).
7 T.W. Schmidt and F.N. Castellano: Photochemical upconversion: the primacy of kinetics. *J. Phys. Chem. Lett.* **5**, 4062 (2014).
8 T.F. Schulze and T.W. Schmidt: Photochemical upconversion: present status and prospects for its application to solar energy conversion. *Energy Environ. Sci.* **8**, 103 (2014).
9 W. Shockley and H.J. Queisser: Detailed balance limit of efficiency of p-n junction solar cells. *J. Appl. Phys.* **32**, 510 (1961).
10 S. Rühle: Tabulated values of the Shockley–Queisser limit for single junction solar cells. *Solar Energy* **130**, 139 (2016).
11 J. Zhou, Q. Liu, W. Feng, Y. Sun, and F. Li: Upconversion luminescent materials: advances and applications. *Chem. Rev.* **115**, 395 (2015).
12 B.D. Ravetz, A.B. Pun, E.M. Churchill, D.N. Congreve, T. Rovis, and L.M. Campos: Photoredox catalysis using infrared light via triplet fusion upconversion. *Nature* **565**, 343 (2019).
13 M. Majek, U. Faltermeier, B. Dick, R. Pérez-Ruiz, and A. Jacobi von Wangelin: Application of visible-to-uv photon upconversion to photoredox catalysis: the activation of aryl bromides. *Chemistry* **21**, 15496 (2015).



https://doi.org/10.1557/mrc.2019.115 Published online by Cambridge University Press

14 M. Häring, R. Pérez-Ruiz, A.J. von Wangelin, and D.D. Díaz: Intragel photoreduction of aryl halides by green-to-blue upconversion under aerobic conditions. *Chem. Commun.* **51**, 16848 (2015).
15 R. Deng, F. Qin, R. Chen, W. Huang, M. Hong, and X. Liu: Temporal full-colour tuning through non-steady-state upconversion. *Nat. Nanotechnol.* **10**, 237 (2015).
16 K.Y. Zhang, T. Zhang, H. Wei, Q. Wu, S. Liu, Q. Zhao, and W. Huang: Phosphorescent iridium(III) complexes capable of imaging and distinguishing between exogenous and endogenous analytes in living cells. *Chem. Sci.* **9**, 7236 (2018).
17 J.P. Mailoa, A.J. Akey, C.B. Simmons, D. Hutchinson, J. Mathews, J.T. Sullivan, D. Recht, M.T. Winkler, J.S. Williams, J.M. Warrender, P.D. Persans, M.J. Aziz, and T. Buonassisi: Room-temperature sub-band gap optoelectronic response of hyperdoped silicon. *Nat. Commun.* **5**, 3011 (2014).
18 D.L. Dexter: A theory of sensitized luminescence in solids. *J. Chem. Phys.* **21**, 836 (1953).
19 L. Nienhaus, J.-P. Correa-Baena, S. Wieghold, M. Einzinger, T.-A. Lin, K. E. Shulenberger, N.D. Klein, M. Wu, V. Bulović, T. Buonassisi, M.A. Baldo, and M.G. Bawendi: Triplet-sensitization by lead halide perovskite thin films for near-infrared-to-visible upconversion. *ACS Energy Lett.* **4**, 888 (2019).
20 S. Wieghold, A.S. Bieber, Z.A. VanOrman, L. Daley, M. Leger, J.-P. Correa-Baena, and L. Nienhaus: Triplet sensitization by lead halide pervoskite thin films for efficient solid-state photon upconversion at subsolar fluxes. *Matter* **1** (2019). doi:10.1016/j.matt.2019.05.026. in press.
21 S. Wieghold, A.S. Bieber, Z.A. VanOrman, and L. Nienhaus: Influence of triplet diffusion on lead halide perovskite-sensitized solid-state upconversion. *J. Phys. Chem. Lett.* **10**, 3806 (2019).
22 S. Amemori, Y. Sasaki, N. Yanai, and N. Kimizuka: Near-infrared-to-visible photon upconversion sensitized by a metal complex with spin-forbidden yet strong S0-T1 absorption. *J. Am. Chem. Soc.* **138**, 8702 (2016).
23 J. Kim, C.Y. Wong, and G.D. Scholes: Exciton fine structure and spin relaxation in semiconductor colloidal quantum dots. *Acc. Chem. Res.* **42**, 1037 (2009).
24 Z.-Q. You and C.-P. Hsu: Theory and calculation for the electronic coupling in excitation energy transfer. *Int. J. Quantum Chem.* **114**, 102 (2014).
25 G.D. Scholes and G. Rumbles: Excitons in nanoscale systems. *Nat. Mater.* **5**, 683 (2006).
26 Z. Huang, X. Li, M. Mahboub, K.M. Hanson, V.M. Nichols, H. Le, M.L. Tang, and C.J. Bardeen: Hybrid molecule–nanocrystal photon upconversion across the visible and near-infrared. *Nano Lett.* **15**, 5552 (2015).
27 K. Okumura, K. Mase, N. Yanai, and N. Kimizuka: Employing core-shell quantum dots as triplet sensitizers for photon upconversion. *Chemistry* **22**, 7721 (2016).
28 M. Wu, D.N. Congreve, M.W.B. Wilson, J. Jean, N. Geva, M. Welborn, T. Van Voorhis, V. Bulović, M.G. Bawendi, and M.A. Baldo: Solid-state infrared-to-visible upconversion sensitized by colloidal nanocrystals. *Nat. Photonics* **10**, 31 (2016).
29 M.V. Kovalenko, L. Manna, A. Cabot, Z. Hens, D.V. Talapin, C.R. Kagan, V. I. Klimov, A.L. Rogach, P. Reiss, D.J. Milliron, P. Guyot-Sionnnest, G. Konstantatos, W.J. Parak, T. Hyeon, B.A. Korgel, C.B. Murray, and W. Heiss: Prospects of nanoscience with nanocrystals. *ACS Nano* **9**, 1012 (2015).
30 Z. Huang and M.L. Tang: Designing transmitter ligands that mediate energy transfer between semiconductor nanocrystals and molecules. *J. Am. Chem. Soc.* **139**, 9412 (2017).
31 N. Geva, J.J. Shepherd, L. Nienhaus, M.G. Bawendi, and T. Van Voorhis: Morphology of passivating organic ligands around a nanocrystal. *J. Phys. Chem. C* **122**, 26267 (2018).
32 L. Nienhaus, M. Wu, N. Geva, J.J. Shepherd, M.W.B. Wilson, V. Bulović, T. Van Voorhis, M.A. Baldo, and M.G. Bawendi: Speed limit for triplet-exciton transfer in solid-state pbs nanocrystal-sensitized photon upconversion. *ACS Nano* **11**, 7848 (2017).
33 Z. Huang, X. Li, M. Mahboub, K.M. Hanson, V.M. Nichols, H. Le, M.L. Tang, and C.J. Bardeen: Hybrid molecule–nanocrystal photon upconversion across the visible and near-infrared. *Nano Lett.* **15**, 5552 (2015).
34 N. Geva, L. Nienhaus, M. Wu, V. Bulovic, M.A. Baldo, T. Van Voorhis, and M.G. Bawendi: A heterogeneous kinetics model for triplet exciton transfer in solid-state upconversion. *J. Phys. Chem. Lett.* **10**, 3147 (2019).
35 M. Mahboub, H. Maghsoudiganjeh, A.M. Pham, Z. Huang, and M.L. Tang: Triplet energy transfer from PbS(Se) nanocrystals to rubrene: the relationship between the upconversion quantum yield and size. *Adv. Funct. Mater.* **26**, 6091 (2016).
36 Y.Y. Cheng, T. Khoury, R.G.C.R. Clady, M.J.Y. Tayebjee, N.J. Ekins-Daukes, M.J. Crossley, and T.W. Schmidt: On the efficiency limit of triplet–triplet annihilation for photochemical upconversion. *Phys. Chem. Chem. Phys.* **12**, 66 (2009).
37 A. Haefele, J. Blumhoff, R.S. Khnayzer, and F.N. Castellano: Getting to the (square) root of the problem: how to make noncoherent pumped upconversion linear. *J. Phys. Chem. Lett.* **3**, 299 (2012).
38 A. Monguzzi, J. Mezyk, F. Scotognella, R. Tubino, and F. Meinardi: Upconversion-induced fluorescence in multicomponent systems: steady-state excitation power threshold. *Phys. Rev. B* **78**, 195112 (2008).
39 T.N. Singh-Rachford and F.N. Castellano: Supra-nanosecond dynamics of a red-to-blue photon upconversion system. *Inorg. Chem.* **48**, 2541 (2009).
40 T.N. Singh-Rachford and F.N. Castellano: Triplet sensitized red-to-blue photon upconversion. *J. Phys. Chem. Lett.* **1**, 195 (2010).
41 T.N. Singh-Rachford and F.N. Castellano: Pd(II) phthalocyanine-sensitized triplet−triplet annihilation from rubrene. *J. Phys. Chem. A* **112**, 3550 (2008).
42 R.R. Islangulov, J. Lott, C. Weder, and F.N. Castellano: Noncoherent low-power upconversion in solid polymer films. *J. Am. Chem. Soc.* **129**, 12652 (2007).
43 D.V. Kozlov and F.N. Castellano: Anti-Stokes delayed fluorescence from metal–organic bichromophores. *Chem. Commun*, 2860 (2004).
44 R.R. Islangulov, D.V. Kozlov, and F.N. Castellano: Low power upconversion using MLCT sensitizers. *Chem. Commun*, 3776 (2005).
45 C.A. Parker, C.G. Hatchard, and B.E. John: Delayed fluorescence from solutions of anthracene and phenanthrene. *Proc. R. Soc. London A* **269**, 574 (1962).
46 S. Boyde, G.F. Strouse, W.E. Jones, and T.J. Meyer: Intramolecular energy transfer in a chromophoro-quencher complex. *J. Am. Chem. Soc.* **111**, 7448 (1989).
47 S.L. Murov, G.L. Hug, and I. Carmichael: *Handbook of Photochemistry* (M. Dekker, New York, NY, 1993).
48 B.R. Henry and W. Siebrand: *Organic Molecular Photophysics* (Wiley, New York, NY, 1973).
49 J. Shi, M.A. Izquierdo, S. Oh, S.Y. Park, B. Milián-Medina, D. Roca-Sanjuán, and J. Gierschner: Inverted energy gap law for the nonradiative decay in fluorescent floppy molecules: larger fluorescence quantum yields for smaller energy gaps. *Org. Chem. Front.* **6**, 1948 (2019).
50 T. Schmidt, E. Gholizadeh, S. Prasad, Z. L. Teh, T. Ishwara, S. Norman, A. J. Petty, J. E. Anthony, and S. Huang: Oxygen-enhanced upconversion of near infrared light from below the silicon band gap. (2019). doi:10.26434/chemrxiv.7834838
51 P. Duan, N. Yanai, and N. Kimizuka: A bis-cyclometalated iridium complex as a benchmark sensitizer for efficient visible-to-UV photon upconversion. *Chem. Commun.* **50**, 13111 (2014).
52 T.N. Singh-Rachford and F.N. Castellano: Low power visible-to-UV upconversion. *J. Phys. Chem. A* **113**, 5912 (2009).
53 W. Zhao and F.N. Castellano: Upconverted emission from pyrene and di-tert-butylpyrene using $Ir(ppy)_3$ as triplet sensitizer. *J. Phys. Chem. A* **110**, 11440 (2006).
54 P.B. Merkel and J.P. Dinnocenzo: Low-power green-to-blue and blue-to-UV upconversion in rigid polymer films. *J. Lumin.* **129**, 303 (2009).
55 F. Deng, J. Blumhoff, and F.N. Castellano: Annihilation limit of a visible-to-UV photon upconversion composition ascertained from transient absorption kinetics. *J. Phys. Chem. A* **117**, 4412 (2013).
56 Z. Huang, X. Li, B.D. Yip, J.M. Rubalcava, C.J. Bardeen, and M.L. Tang: Nanocrystal size and quantum yield in the upconversion of green to violet light with CdSe and anthracene derivatives. *Chem. Mater.* **27**, 7503 (2015).
57 A. Ronchi, P. Brazzo, M. Sassi, L. Beverina, J. Pedrini, F. Meinardi, and A. Monguzzi: Triplet-triplet annihilation based photon up-conversion in



https://doi.org/10.1557/mrc.2019.115 Published online by Cambridge University Press

hybrid molecule–semiconductor nanocrystal systems. *Phys. Chem. Chem. Phys.* **21**, 12353 (2019).
58 C. Mongin, S. Garakyaraghi, N. Razgoniaeva, M. Zamkov, and F.N. Castellano: Direct observation of triplet energy transfer from semiconductor nanocrystals. *Science* **351**, 369 (2016).
59 J. Lauth, G. Grimaldi, S. Kinge, A.J. Houtepen, L.D.A. Siebbeles, and M. Scheele: Ultrafast charge transfer and upconversion in zinc β-tetraaminophthalocyanine-functionalized PbS nanostructures probed by transient absorption spectroscopy. *Angew. Chem.* **129**, 14249 (2017).
60 M. Mahboub, H. Maghsoudiganjeh, A.M. Pham, Z. Huang, and M.L. Tang: Triplet energy transfer from PbS(Se) nanocrystals to rubrene: the relationship between the upconversion quantum yield and size. *Adv. Funct. Mater.* **26**, 6091 (2016).
61 Z. Huang, Z. Xu, M. Mahboub, Z. Liang, P. Jaimes, P. Xia, K.R. Graham, M.L. Tang, and T. Lian: Enhanced near-infrared-to-visible upconversion by synthetic control of PbS nanocrystal triplet photosensitizers. *J. Am. Chem. Soc.* **141**, 9769 (2019).
62 A.C.S. Samia, X. Chen, and C. Burda: Semiconductor quantum dots for photodynamic therapy. *J. Am. Chem. Soc.* **125**, 15736 (2003).
63 E.I. Zenkevich, E.I. Sagun, V.N. Knyukshto, A.S. Stasheuski, V.A. Galievsky, A.P. Stupak, T. Blaudeck, and C. von Borczyskowski: Quantitative analysis of singlet oxygen ($^1O_2$) generation via energy transfer in nanocomposites based on semiconductor quantum dots and porphyrin ligands. *J. Phys. Chem. C* **115**, 21535 (2011).
64 N.J. Thompson, M.W.B. Wilson, D.N. Congreve, P.R. Brown, J.M. Scherer, T.S. Bischof, M. Wu, N. Geva, M. Welborn, T.V. Voorhis, V. Bulović, M.G. Bawendi, and M.A. Baldo: Energy harvesting of non-emissive triplet excitons in tetracene by emissive PbS nanocrystals. *Nat. Mater.* **13**, 1039 (2014).
65 M. Tabachnyk, B. Ehrler, S. Gélinas, M.L. Böhm, B.J. Walker, K.P. Musselman, N.C. Greenham, R.H. Friend, and A. Rao: Resonant energy transfer of triplet excitons from pentacene to PbSe nanocrystals. *Nat. Mater.* **13**, 1033 (2014).
66 L. Nienhaus, M. Wu, V. Bulović, M.A. Baldo, and M.G. Bawendi: Using lead chalcogenide nanocrystals as spin mixers: a perspective on near-infrared-to-visible upconversion. *Dalton Trans.* **47**, 8509 (2018).
67 K. Mase, K. Okumura, N. Yanai, and N. Kimizuka: Triplet sensitization by perovskite nanocrystals for photon upconversion. *Chem. Commun.* **53**, 8261 (2017).
68 M. Mahboub, Z. Huang, and M.L. Tang: Efficient infrared-to-visible upconversion with subsolar irradiance. *Nano Lett.* **16**, 7169 (2016).
69 Y. Liu, M. Gibbs, J. Puthussery, S. Gaik, R. Ihly, H.W. Hillhouse, and M. Law: Dependence of carrier mobility on nanocrystal size and ligand length in PbSe nanocrystal solids. *Nano Lett.* **10**, 1960 (2010).
70 M. Wu, J. Jean, V. Bulović, and M.A. Baldo: Interference-enhanced infrared-to-visible upconversion in solid-state thin films sensitized by colloidal nanocrystals. *Appl. Phys. Lett.* **110**, 211101 (2017).
71 X. Luo, R. Lai, Y. Li, Y. Han, G. Liang, X. Liu, T. Ding, J. Wang, and K. Wu: Triplet energy transfer from $CsPbBr_3$ nanocrystals enabled by quantum confinement. *J. Am. Chem. Soc.* **141**, 4186 (2019).
72 Y. Han, X. Luo, R. Lai, Y. Li, G. Liang, and K. Wu: Visible-light-driven sensitization of naphthalene triplets using quantum-confined $CsPbBr_3$ nanocrystals. *J. Phys. Chem. Lett.* **10**, 1457 (2019).
73 R. Younts, H.-S. Duan, B. Gautam, B. Saparov, J. Liu, C. Mongin, F.N. Castellano, D.B. Mitzi, and K. Gundogdu: Efficient generation of long-lived triplet excitons in 2D hybrid perovskite. *Adv. Mater.* **29**, 1604278 (2017).
74 Y. Yang, M. Yang, Z. Li, R. Crisp, K. Zhu, and M.C. Beard: Comparison of recombination dynamics in $CH_3NH_3PbBr_3$ and $CH_3NH_3PbI_3$ perovskite films: influence of exciton binding energy. *J. Phys. Chem. Lett.* **6**, 4688 (2015).
75 K. Galkowski, A. Mitioglu, A. Miyata, P. Plochocka, O. Portugall, G.E. Eperon, J.T.-W. Wang, T. Stergiopoulos, S.D. Stranks, H.J. Snaith, and R.J. Nicholas: Determination of the exciton binding energy and effective masses for methylammonium and formamidinium lead tri-halide perovskite semiconductors. *Energy Environ. Sci.* **9**, 962 (2016).
76 A. Miyata, A. Mitioglu, P. Plochocka, O. Portugall, J.T.-W. Wang, S.D. Stranks, H.J. Snaith, and R.J. Nicholas: Direct measurement of the exciton binding energy and effective masses for charge carriers in organic–inorganic tri-halide perovskites. *Nat. Phys.* **11**, 582 (2015).
77 W. Tress: Perovskite solar cells on the way to their radiative efficiency limit—insights into a success story of high open-circuit voltage and low recombination. *Adv. Energy Mater.* **7**, 1602358 (2017).
78 L. Nienhaus, N. Geva, J. Correa-Baena, M. Wu, S. Wieghold, V. Bulović, T. V. Voorhis, M. A. Baldo, T. Buonassisi, and M. G. Bawendi: In 2018 *IEEE 7th World Conference on Photovoltaic Energy Conversion (WCPEC) (A Joint Conference of 45th IEEE PVSC, 28th PVSEC 34th EU PVSEC)*, Waikoloa Village, Hawaii; 2018; pp. 3698–3702.
79 P.D. Reusswig, D.N. Congreve, N.J. Thompson, and M.A. Baldo: Enhanced external quantum efficiency in an organic photovoltaic cell via singlet fission exciton sensitizer. *Appl. Phys. Lett.* **101**, 113304 (2012).
80 T.R. Kafle, B. Kattel, S.D. Lane, T. Wang, H. Zhao, and W.-L. Chan: Charge transfer exciton and spin flipping at organic–transition-metal dichalcogenide interfaces. *ACS Nano* **11**, 10184 (2017).
81 T.R. Kafle, B. Kattel, P. Yao, P. Zereshki, H. Zhao, and W.-L. Chan: Effect of the interfacial energy landscape on photoinduced charge generation at the ZnPc/$MoS_2$ interface. *J. Am. Chem. Soc.* **141**, 11328 (2019).



https://doi.org/10.1557/mrc.2019.115 Published online by Cambridge University Press